Vorticity Suppression by Multiphase Effects in Shock-Driven Variable Density Mixing

Vasco Duke-Walker^a, Jacob A. McFarland^a

^aTexas A&M University, 3123 TAMU, College Station, 77843, Texas, United States

Abstract

Shock-driven variable density mixing has been frequently explored through the single-phase Richtmyer-Meshkov instability. Here, such mixing is considered when driven by a multiphase component, the Shock-Driven Multiphase Instability (SDMI). The simple case of a solid particle seeded gas in a cylindrical region surrounded by clean gas is studied. It has been previously shown that the particle-phase can lag behind the gas, diminishing vorticity deposition. In this letter we present theoretical analysis of the vorticity deposition, and a new model predicting the circulation deposition for an SDMI as a function of particle relaxation distance and hydrodynamic mixing strength. The theory is founded on a simplified vorticity equation, advection and multiphase source terms, using simple drag models to predict the particle dynamics, and scaling the results using existing circulation models for the Richtmyer-Meshkov instability in the small particle limit. The model is compared to new high-fidelity experimental data, and previous experiments and simulations, finding good agreement. This model provides the first theoretical prediction of mixing suppression in the SDMI.

Keywords: Multiphase mixing, Richtymer-Meshkov Instability *PACS:* 47.55.-t, 47.35.-i, 47.51.+a

The instantaneous acceleration of a perturbed variable-density fluid inter-

face by a shock wave results in strong vorticity ω deposition and subsequent

mixing (fig. 1). When both fluids are continuous and of a single phase, the resulting hydrodynamic instability is known as the Richtmyer-Meshkov

instability (RMI). The RMI has been well-studied for its applications in in-

⁶ ertial confinement fusion and combustion among others. A closely related

⁷ instability, the Shock-Driven Multiphase Instability (SDMI), results when

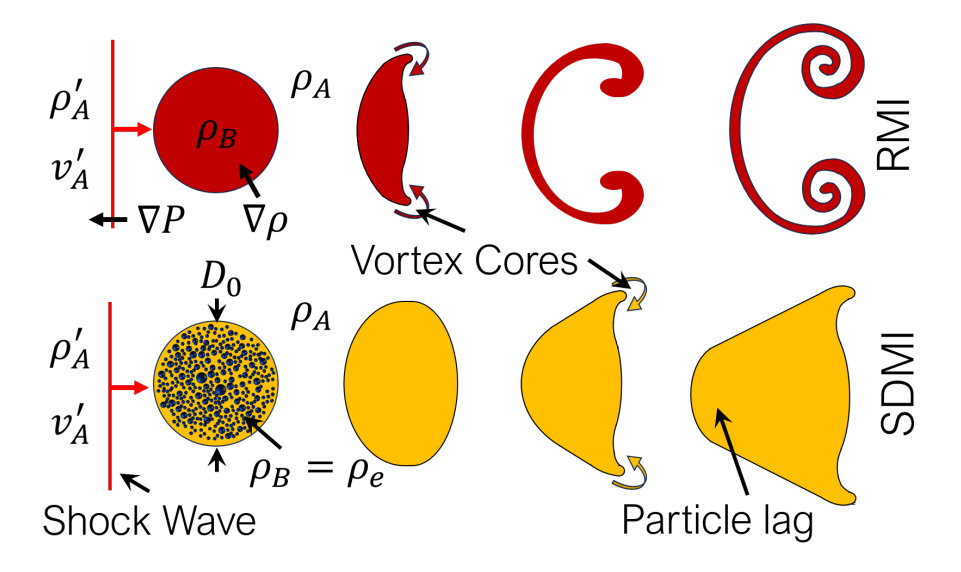


Figure 1: The development of the Richmyer-Meshkov and Shock-Driven Multiphase Instabilities highlighting the effect of particle lag.

one or both fluids is composed of a multiphase mixture, e.g. particles and gas. If the coupling of the phases is slow relative to the hydrodynamic time scales, then one phase will lag behind the other. These lag effects have been observed to reduce the shock-deposited vorticity at the interface while also increasing particle entrainment. This letter, and the supporting document [7], study the vorticity deposition on a cylindrical SMDI interface, a problem frequently arising in combustion applications. Theory for multiphase effects and a model to predict the circulation deposition, based on RMI models and particle momentum equilibration rates, is presented.

16

In the RMI, vorticity is deposited due to a misalignment between pressure and density gradients. This misalignment creates baroclinic vorticity along the fluid interface as seen in the vorticity eqn 1, where u_i is the gas velocity, ρ_g in the gas density, τ_{jl} is the viscous stress tensor, and B_j is a body force. The pressure gradient is often characterized by the shock wave Mach number while the density gradient is characterized by the gas Atwood number $A_g = (\rho_B - \rho_A)/(\rho_B + \rho_A)$, where ρ_A and ρ_B are the initial density of the surrounding and interface gases respectively.

$$\partial_t \omega_k + u_j \partial_j \omega_i = \omega_j \partial_j u_i - \omega_i \partial_j u_j + \underbrace{\frac{1}{\rho_g^2} \varepsilon_{kij} \partial_i \rho_g \partial_j P}_{\text{baroclinic}} + \varepsilon_{kij} \partial_i \frac{\partial_l \tau_{jl}}{\rho_g} + \underbrace{\varepsilon_{kij} \partial_i \frac{B_j}{\rho_g}}_{\text{body force}}.$$
(1)

26

35

The misalignment of pressure and density gradients frequently results from a perturbation in the fluid interface. While linear stability theory treats the interface perturbation by means of a Fourier series (sine waves), circular and spherical interface geometries are common in many applications, e.g. fuel jets and bubbles [19]. Several models have been proposed to predict RMI circulation ($\Gamma = \int \omega dA$) deposition on cylindrical interfaces. Wang et al. [18] provides a summary and comparison of these models. The model of Picone and Boris [13], of interest in this work, predicts the circulation as shown in eqn. 2.

$$\Gamma_{PB} = v_A' \left(\frac{v_A'}{w_i} - 2 \right) \frac{D_0}{2} * ln(\rho_B/\rho_A)$$
 (2)

In the case of the SDMI, RMI theory can be applied by treating the multiphase mixtures as single fluids with appropriately averaged properties. An effective density ρ_e for the interface fluid can be found as the sum of gas and particle mass divided by the total volume in the interface. The effective Atwood number can then be found as $A_e = (\rho_e - \rho_A)/(\rho_e + \rho_A)$. Using the effective interface density, RMI theory provides a good prediction of SDMI circulation in the case of small fast reacting particles. As particles become larger, or heavier, their velocity equilibration time (t_v) becomes significant compared to the hydrodynamic time scale, taken as $t_h = D_0/w_i$, where D_0 in the interface length scale (diameter) and w_i is the incident shock wave velocity. The non-dimension relation time then is $\tau_v = t_v/t_h$.

The particles generate a drag force on the gas that generates vorticity through the body force term (eqn. 1). As the particles advect through the gas, they carry the vorticity production term, depositing vorticity over their path. This leads to increased dissipation of the newly deposited vorticity, resulting in decreased circulation. Dahal and McFarland proposed that this misalignment could be understood through enstrophy, eqn. 3, where $\Omega = \omega_k \omega_k/2$. In this equation, the multiphase enstrophy production can be seen to increase when the enstrophy source term and previously deposited vorticity are aligned.

$$D_t\Omega =$$

57

58

77

$$\frac{\omega_{i}\omega_{j}\partial_{j}u_{i} - \omega_{i}\omega_{i}\partial_{j}u_{j} + \underbrace{\frac{\omega_{k}}{\rho_{g}^{2}}\varepsilon_{kij}\partial_{i}\rho_{g}\partial_{j}P}_{\text{baroclinic}} + \nu\partial_{j}\partial_{j}\Omega - \nu\partial_{j}\omega_{i}\partial_{j}\omega_{i} + \underbrace{\omega_{k}\varepsilon_{kij}\partial_{i}\frac{B_{j}}{\rho_{g}}}_{\text{multiphase}} (3)$$

The SDMI was first shown experimentally by Vorobieff et al. [16]. Subsequent work by McFarland et al. [10] found that instability could result from differences in both effective densities and equilibration times. Dahal and McFarland [4] suggested that circulation deposition was reduced due to the misalignment of vorticity deposited by the advecting particle field and the gas phase vorticity. Middlebrooks et al. [11] highlighted the effects of droplet size and breakup in experiments, while Duke et al. [6] simulated these experiments and provided further insight into the effect of breakup and evaporation on the SDMI. Si et al. [15] explored the effect of Stokes number, St, on a combined RMI and SMDI in simulations.

The degree of momentum coupling between particles and gas is determined from the drag force and particle mass. In the absence of deformation or breakup, the particle can be treated as a simple sphere with diamter d_p . Various forces arise on the particle [9] during shock interaction, but among these the steady drag force is the most influential [1]. The drag force depends on the time-dependent Reynolds number $(Re = \rho'_B d_p(v'_A - v_p)/\mu'_B)$, where ρ'_B is the post shock carrier gas density, v_p is the particle velocity relative to the gas, μ'_B the post-shock carrier gas viscosity, and v'_A is the carrier gas post-shock velocity. Here we assume $v'_A \approx v'_B$ as the interface gas is limited in size (mass) and will equilibrate with the surrounding gas velocity.

For low Re, the Stokes flow drag relation can be used, $C_D = 24/Re$. It is assumed that equilibrium is achieved when the final velocity of the particle reaches 99% of the freestream gas velocity, $v_{p,f} = 0.99v_A'$, transferring 98% of its momentum to the gas phase. From the Stokes drag force, the particle velocity equilibration time can be found as $t_{v,s} = -ln(0.01)/B$, where $B = 18\mu_B'/(d_p^2\rho_p/)$ and ρ_p is the density of the particle material. The distance the particle travels relative to the gas at this time, the lag distance, can be found as $x_{f,s} = -v_A'/B(e^{-Bt} - 1)$.

At higher Re, various models have been proposed. Cloutman [3] provided an analytical solution for particle trajectories based on the Kliatchko drag model (eqn. 4). Only the Re < 1000 solutions are presented as the particles

and conditions used here meet this criteria. The high Re velocity equilibration time can be found as shown in eqn. 5, where $C = \frac{1}{6}[d_p \rho_g/(\mu)]^{2/3}$. The lag distance, can be found by eqn. 6.

92

93

$$C_D = \begin{cases} 24/Re + 4/Re^{1/3} & Re \le 1000\\ 0.424 & Re > 1000 \end{cases}$$
 (4)

$$t_{v,c} = \frac{3}{2B} ln \left(\frac{v_{p,f}^{-2/3} + C}{v_A^{\prime - 2/3} + C} \right)$$
 (5)

$$x_{l,c} = \frac{3}{BC} \left(v_A^{\prime \frac{1}{3}} + C^{-\frac{1}{2}} \arctan C^{-\frac{1}{2}} v_A^{\prime -\frac{1}{3}} - v_{p,f}^{\frac{1}{3}} - C^{-\frac{1}{2}} \arctan C^{-\frac{1}{2}} v_{p,f}^{-\frac{1}{3}} \right)$$

$$(6)$$

To study the SDMI, a cylindrical multiphase interface was created in a shock tube facility (fig.2) with internal cross section of $\approx 14x14cm$, following the methods of Duke et al. [5]. The carrier and surrounding gas were air initially at ambient conditions ($T=293K,\ P=100.3kPa$). A Mach 1.35 ± 0.007 shock wave was used to accelerate the interface, providing repeatability, and sufficient hydrodynamic time scales for imaging. Shock wave velocities and pressures were measured by dynamic pressure transducers and gas properties calculated from gas dynamics equations ($v_A'=177.4\pm3.3m/s$, $\rho_B'=1.9\pm0.01kg/m^3$).

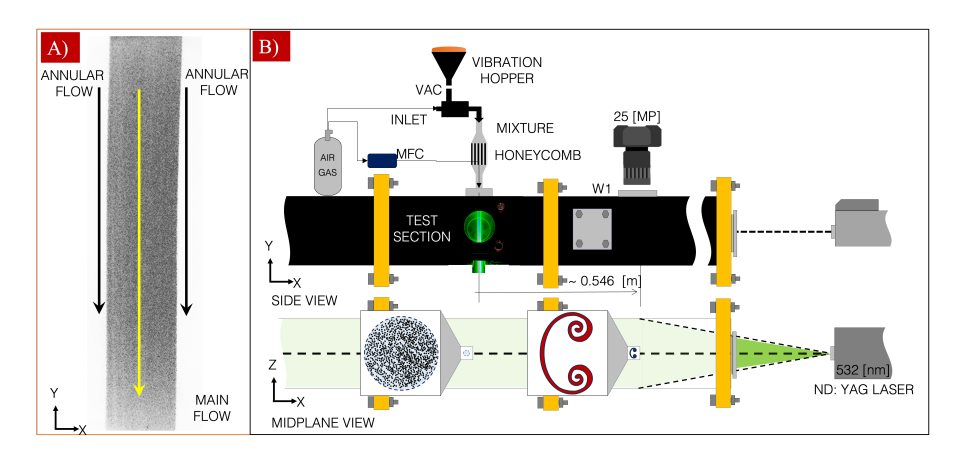


Figure 2: Shock Tube facility, interface Initial Conditions and Diagnostics: A) example of the stability of the multiphase interface, and B) test section configuration

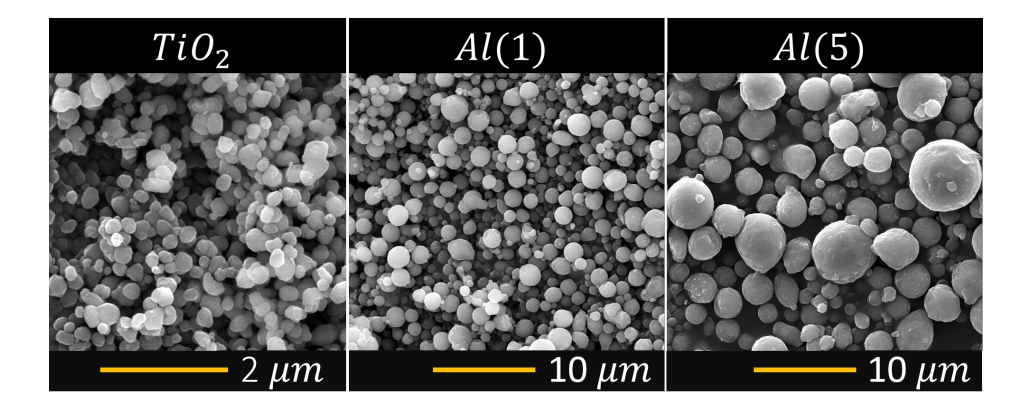


Figure 3: Scanning Electron Microscopy images of the particles used. Note the scale is different for the smallest particles.

Solid particles were used in place of the previous liquid droplets to avoid deformation and breakup effects. Following the results of McFarland et al. [10], particles with $\tau_v = \mathcal{O}(0.1,1,10)$ were desired. TiO_2 particles $(4200kg/m^3)$ with nominal diameter of $0.2\mu m$ and aluminum particles $(\rho_{Al} = 2700kg/m^3)$ with nominal diameters of 1 and 5 μm were used.

Particle sizes were measured ex-situ via scanning electron microscopy (fig. 3) and in-situ via phase Doppler Particle Anemometry (PDPA). Table 1 provides the sizes measured, though the TiO_2 particles were below the detectable range for PDPA. The arithmetic mean diameter (d_{10}) agreed, but the PDPA measurement found larger Sauter mean diameters (d_{32}) . We attribute this discrepancy to agglomeration that may occur in the delivery of the particles to the shock tube.

Table 1: Particle size statistics

PI		TiO_2	Al(1)	Al(5)
SEM	$D_{10}[\mu m]$	0.2	1.18	4.61
SEW	$D_{32}[\mu m]$	0.3	1.65	6.28
PDPA 120 mm	$D_{10}[\mu m]$	-	1.56	4.30
	$D_{32}[\mu m]$	_	2.31	9.73

A solid particle delivery system consisting of a vibrating hopper, ejector pump, and flow-straightener was used to create a cylindrical interface with $D_0 = 1.24 \pm 0.01 cm$, as seen in fig.2. The particle mass flow rate was measured in-situ by capturing, filtering, and weighing (balance accuracy of

 $\pm 0.1[mg]$) the particles exiting the interface creation device over a 1 minute time. Particle mass flow rates were consistent such that the gas flow rates could be adjusted to provide $A_e = 0.0379 \pm 0.009$.

Three cases (table 2) were developed to study the desired range of τ_v . For case 1, it was desired to have $(\tau_v \approx 0)$, essentially an RMI. The TiO_2 particles were found to provide a sufficiently low lag distances to act as a reliable gas tracer. Thus, A_e was set by using a gas mixture $(80/20\%-N_2/CO_2)$ by volume, $\rho_B = 1.28kg/m^3$) with the particles contributing a negligible mass to the interface. For cases 2 and 3, the aluminum particles were seeded in air. Temperatures were monitored $(T_A/T_B = 1.00 \pm 0.02)$ to ensure that the carrier and surrounding gas densities matched and did not contribute to A_e .

Table 2: Initial conditions

cases	1	2	3
Particles	TiO_2	Al(1)	Al(5)
τ_v for d_{10}	0	1.27	2.54
τ_v for d_{32}	0	7.37	28.3
A_g	0.0388	0	0
A_e	0.0388	0.0376	0.0371
σ_{A_e}	0.0001	0.0086	0.0074

The interface development was imaged by laser Mie-scattering. A laser sheet (< 0.2cm thick by 2cm wide) created by a pulsed dual head Nd:YAG laser (532nm, 150mj/pulse) is introduced through a window at the end of the shock tube. The sheet and cameras are oriented to allow the $r\Theta$ plane of the cylinder to be imaged. Cameras (La Vision 25MP CMOS) are mounted at two windows to view the initial interface and its evolution at a downstream location ($\approx 0.546m$) with resolution up to $\sim 6\mu m/px$. The cameras and laser are triggered by an upstream pressure transducer.

To acquire particle velocities, the particle imaging velocimetry (PIV) technique was used. Two images were acquired with laser pulses triggered $2\mu s$ apart. The DaVIS 11.0 software was used to correlate the images and provided a velocity field with a 24 x 24 pixel spacing with a 50% overlap. A multi-pass cross correlation was used, with the final pass providing vectors with $\approx 72\mu m$ spatial resolution. The vectors were post-processed to reduce noise and a Gaussian smoothing filter applied to smooth gradients. It should be noted that PIV is challenging in shock-driven flows and at high particle concentrations [12]. The velocity measurements obtained are for

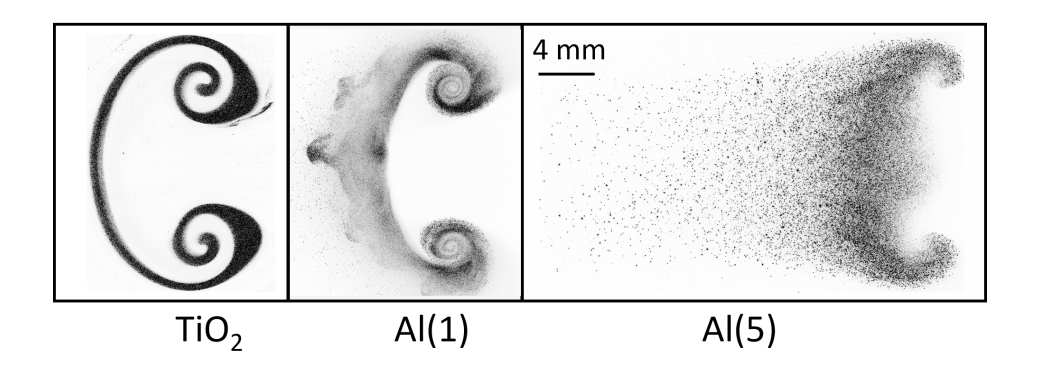


Figure 4: Interface development for each case at $t \approx 3ms$.

the particle phase and only provide an estimate of the gas velocity once in equilibrium. The supporting document [7] provides more details on the experimental methods.

Figure 4 shows the late-time evolution of the interface for each case at $t \approx 3ms$. Case 1 (RMI) shows well-developed vortex cores similar to observations in previous RMI works [14]. Case 2 shows a more perturbed development with secondary instabilities arising on the upstream (left) interface. The particle field is more diffused in the vortex cores dues to lag effects. Case 3 shows much less development of the vortex cores and a long tail of larger particles lagging behind the flow (left). It is notable that the development of these cases follows closely the trends shown in early SDMI simulations [4, 17].

Vorticity (ω_z) fields were found by first-order finite difference method for each case as shown in fig. 5. It should be noted that at this late time the particles have equilibrated with the gas flow, thus the particles should be an accurate tracer of gas velocity where present. While well-defined vortex cores are visible, each case also shows spurious alternating patches of positive and negative vorticity along the upstream portion of the interface.

To determine the circulation the center of each vortex core is first identified by the location of maximum swirling strength. A line integral of the azimuthal velocity field is performed along a circle centered on the vortex core ($\oint \vec{v} \cdot \vec{dr}$). The radius of this circle is increased until the maximum circulation is found, as seen in figure 6. This procedure was repeated for 8-10 images for each case to determine the average circulation. It should be noted that this method produces a conservative estimate as it excludes some

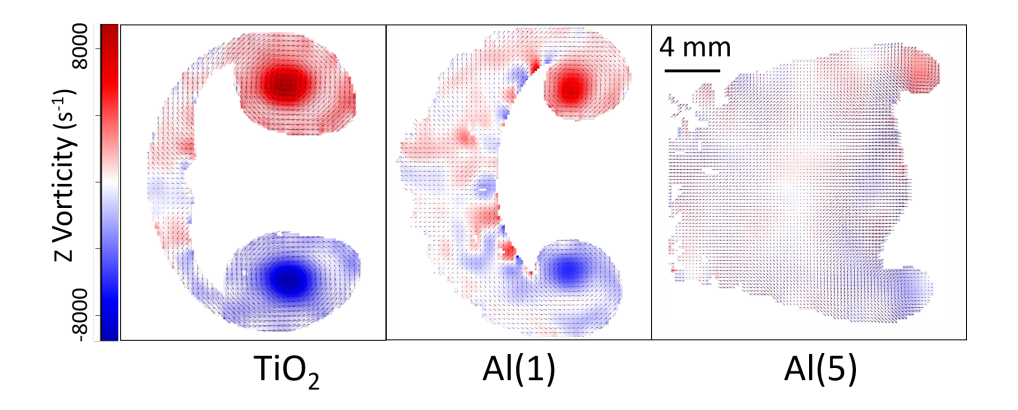


Figure 5: Vorticity for each case at $t \approx 3ms$.

of the vorticity outside the cores. Furthermore, some vorticity present in the carrier gas is missed, due to the absence of tracer particles in this gas. This is most significant for case 1, where there is little diffusion of particles across the interface. Table 3 shows the average circulation found for each case.

Table 3: Average and standard deviation of circulation (cm^2/s) from vortex cores

Cases	1	2	3
Γ	952.45	320.75	56.159
$\sigma_{\Gamma}\pm$	98.078	116.46	22.85

176

178

179

180

184

186

The circulation for the RMI case can be predicted by various models, but the one provided by Picone and Boris (PB, eqn. 2) has been shown to perform well for heavy gas cylinders [18]. From this model, case 1 should have a circulation of $\Gamma_{PB} = 1350cm/s^2$. Using this value we plot a normalized circulation Γ/Γ_{PB} versus the characteristic particle diameter (d_c) in figure 7. We use the d_{32} value for d_c as the lag distance scales with d^2 while the momentum carried by each particle scales with d^3 . Data from previous experimental and simulation works on circular SDMI interfaces are included as well. In order to scale d_c for different particle materials from previous works, we take d_c to be for aluminum particles, scaling other materials as $d_c = d_{32}(\rho_p/\rho_{Al})$.

As proposed in Dahal and McFarland [4], vorticity should be a function of both the strength of particle source term and its alignment with the gas phase. To explain the observed circulation deposition we propose a simplified

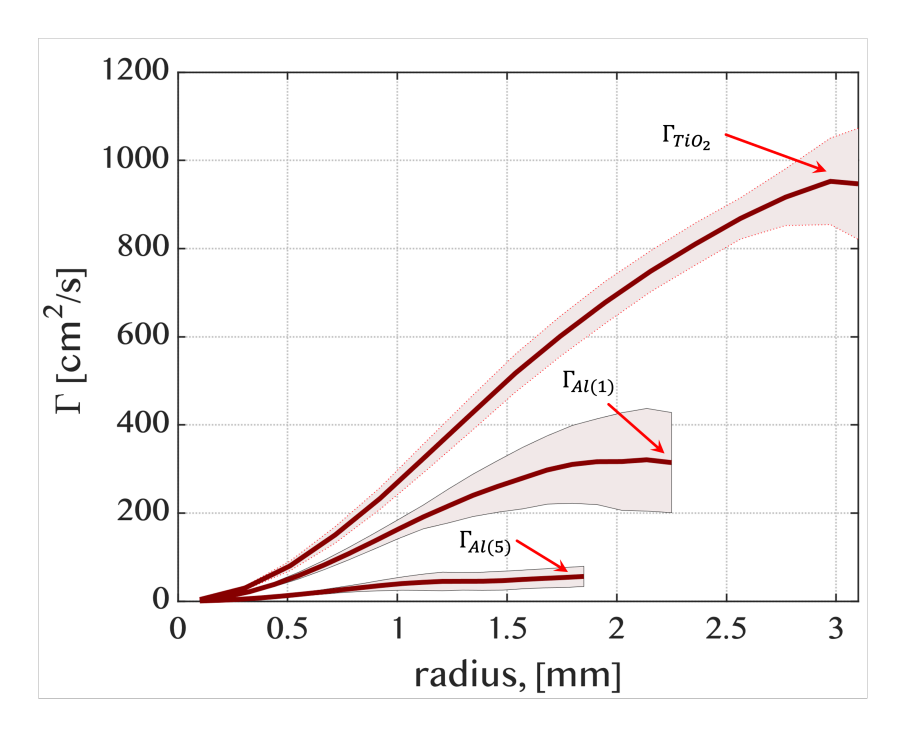


Figure 6: Circulation estimate versus circle radius for the evaluation of the line integral. The center line represents the average and the shaded region the maximum and minimum for all trials.

model based on the vorticity and enstrophys equations (eqns. 1 and 3). For this problem the flowfield can be taken to be 2D and incompressible (post-shock), with gas velocity and momentum source term primarily in the x-direction. The enstrophy can be found for a control volume (CV) that travels with the particles as seen in eqn. 7, where ω_l is the vorticity local to the CV given in eqn. 8, B_x is the momentum source term, and v_x the gas velocity relative to the particles.

191

193

195

197

198

199

$$D_t \Omega = \frac{1}{\rho_B'} \omega_l \partial_y B_x \tag{7}$$

$$\partial_t \omega_l = \frac{1}{\rho_B'} \partial_y B_x - v_x \partial_x \omega_l \tag{8}$$

A closed-form solution for ω_l and Ω can be found for the Stokes drag model, $B_x = m_p B x'(t)$ where m_p is the total particle mass in the cloud. The length scale for the CV is taken as the radius of the interface, $D_0/2$, and was found to well-represent the length scale for the interface vorticity. By numerical integration [7], it was found that the Stokes and Cloutman solutions provide similar ($\pm 10\%$) vorticity deposition at particles sizes less than $\sim 2.5\mu m$. At $10\mu m$, approximately the Al(5) case d_{32} , the error increases to near 300%. While this error is significant, both models result in a similar trends with particle size and predict much lower vorticity for larger particles.

The final vorticity is obtained as $t \to \infty$, when the Stokes lag distance reaches its maximum value, x_s . The maximum vorticity is found as $d_p \to 0$, e.g. $\lim_{x_s\to 0} \omega(x_s)$. Taking that circulation is proportional to vorticity and should approach that of an RMI at this maximum(eqn. 2), equations 7 and 8 can be solved with the Stokes drag model and scaled to predict circulation for the circular interface as shown in equations 9 and 10.

$$\Gamma_t = \sqrt{2}B \left(\frac{D_0}{2}\right)^2 ln \left(\frac{\rho_e}{\rho_B'}\right) \left(\frac{v_A'}{w_i} - 2\right) * \left(\frac{2}{D_0}x_f + e^{-2x_f/D_0} - 1\right)^{1/2}$$
(9)

$$\Gamma_l = B\left(\frac{D_0}{2}\right)^2 ln\left(\frac{\rho_e}{\rho_B'}\right) \left(\frac{v_A'}{w_i} - 2\right) \left(1 - e^{-2x_f/D_0}\right) \tag{10}$$

These equations are normalized by the maximum circulation (Γ_{PB}), and plotted in fig. 7. We attribute the disagreement in circulation for case 1 to a lack of vorticity information in the surrounding gas and a limited measurement resolution. Simulation results for small particles [4] showed better agreement with the models. The simulations from Duke et al. (2021) [6] also showed a lower circulation than predicted by either model for small particles. We believe this is due to initial water vapor in the interface, creating a small negative A_g .

At larger diameters, experimental data from Duke et al. (2020) [5] shows a higher circulation than predicted by the Γ_l model. In this experiment, a significant positive A_g was present increasing the gas phase vorticity, which is not captured in the current models. Also, the droplets underwent a breakup process, reducing their equilibration time. Simulations from Duke et al. (2021) [6] also show an increased circulation deposition for large particle sizes. This again can be attributed to droplet breakup decreasing the effective equilibration time. Another source of error for large particle cases is that the particles lag behind even small gas velocity changes, and thus the PIV measurements may show less circulation than that of the gas phase.

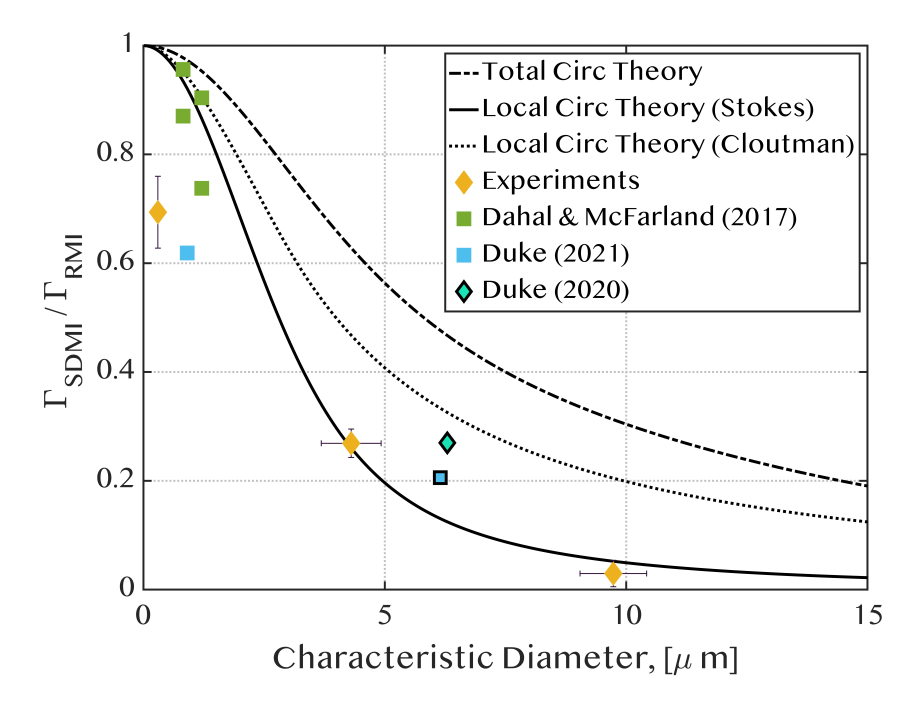


Figure 7: Circulation versus particle characteristic size. Blue line: Circulation predicted by theory. Orange squares: Current experimental data. Green circles: Simulations from [4]. Blue circles: Simulations from [6]. Yellow square: Experiments of [5]. Red outlines indicate data with breakup effects.

Overall the local circulation model shows better agreement for larger particles sizes than the total circulation model. The reason for this is primarily due to the dissipation of advected vorticty, that is not captured in eqn. 9. Vorticity advected downstream is dissipated by viscous effects. In the case of the simulation results, advected vorticity is dissipated through numerical viscosity and diffusion. It should also be noted that other drag models may be applied, and those developed for the Re found in this work (e.g. [2, 8]) produce similar results.

The local circulation model provides a new theoretical understanding for the effect of finite momentum coupling rates on the SDMI. The model makes several fundamental assumptions: 1) The advection and multiphase source terms dominate the interface vorticity dynamics, 2) In the small-particle limit the circulation reaches that of an equivalent RMI, 3) The circulation decreases as the particle lag distance increases relative to the interface vorticity length scale, $D_0/2$ here 4) The particle lag distance is a function of the drag force, modeled here by the steady drag for a simple sphere in isolation.

With these assumptions, the theory can be easily generalized to other interface geometries by scaling with the appropriate circulation and drag models. The results suggest that mixing suppression by multiphase effects can be predicted and perhaps exploited in engineering applications, such as inertial confinement fusion (ICF) and shock-driven combustion. Future work will explore the effect of including the baroclinic term for interfaces with gas phase density differences, providing further insight into droplet laden fuel vapor mixing and particle laden gas/plasma interfaces such as those found in ICF and supernovae.

This work was supported by the National Science Foundation, United States through award number 2053154. The authors would like to thank Manoj Paudel for his helpful discussion of the results.

262 References

- [1] Capecelatro, J., Wagner, J.L., 2024. Gas-particle dynamics in high-speed flows. Annual Review of Fluid Mechanics 56, 379–403.
- ²⁶⁵ [2] Clift, R., Gauvin, W., 1971. Motion of entrained particles in gas streams. The Canadian Journal of Chemical Engineering 49, 439–448.
 - [3] Cloutman, L.D., 1988. Analytical solutions for the trajectories and ther-

- mal histories of unforced particulates. American Journal of Physics 56, 643–645.
- ²⁷⁰ [4] Dahal, J., McFarland, J.A., 2017. A numerical method for shock driven multiphase flow with evaporating particles. Journal of Computational Physics 344, 210–233.
- [5] Duke-Walker, V., Allen, R., Maxon, W.C., McFarland, J.A., 2020. A
 method for measuring droplet evaporation in a shock-driven multiphase
 instability. International Journal of Multiphase Flow 133, 103464.
- [6] Duke-Walker, V., Maxon, W.C., Almuhna, S.R., McFarland, J.A., 2021.
 Evaporation and breakup effects in the shock-driven multiphase instability. Journal of Fluid Mechanics 908, A13.
- ²⁷⁹ [7] Duke-Walker, V.O., McFarland, J.A., 2024. Vorticity suppression by particle lag effects in shock-driven multiphase instability. arXiv:2405.00111.
- [8] Ingebo, R.D., 1956. Drag coefficients for droplets and solid spheres in clouds accelerating in airstreams.

 Technical Report.
- [9] Maxon, W.C., Nielsen, T., Denissen, N., Regele, J.D.,
 McFarland, J., 2021. A high resolution simulation of
 a single shock-accelerated particle. Journal of Fluids
 Engineering 143, 071403.
- [10] McFarland, J.A., Black, W.J., Dahal, J., Morgan, B.E., 290 2016. Computational study of the shock driven instability 291 of a multiphase particle-gas system. Physics of Fluids 28.
- [11] Middlebrooks, J.B., Avgoustopoulos, C.G., Black, W.J., Allen, R.C., McFarland, J.A., 2018. Droplet and multiphase effects in a shock-driven hydrodynamic instability with reshock. Experiments in Fluids 59, 1--16.
- 296 [12] Orlicz, G.C., Balasubramanian, S., Vorobieff, P., 297 Prestridge, K.P., 2015. Mixing transition in a shocked 298 variable-density flow. Physics of Fluids 27.

- 299 [13] Picone, J., Boris, J., 1988. Vorticity generation by shock 300 propagation through bubbles in a gas. Journal of Fluid 301 Mechanics 189, 23--51.
- [14] Ranjan, D., Oakley, J., Bonazza, R., 2011. Shock-bubble interactions. Annual Review of Fluid Mechanics 43, 117--140.
- [15] Si, Y., Li, S., Meng, B., Wang, C., Tian, B., 2024. A
 dominant dimensionless number and theoretical model for
 the evolution of multiphase richtmyer--meshkov instability.
 Physics of Fluids 36.
- [16] Vorobieff, P., Anderson, M., Conroy, J., White, R., Truman, C.R., Kumar, S., 2011. Vortex formation in a shock-accelerated gas induced by particle seeding. Physical review letters 106, 184503.
- [17] Vorobieffl, P., Anderson, M., Conroy, J., Truman, C.R., Kumar, S., 2013. Morphology of shock-accelerated multiphase flow: experiment and modeling. Computational Methods in Multiphase Flow VII 79, 15.
- [18] Wang, X., Yang, D., Wu, J., Luo, X., 2015. Interaction of a weak shock wave with a discontinuous heavy-gas cylinder.

 Physics of Fluids 27.
- [19] Yang, J., Kubota, T., Zukoski, E.E., 1994. A model for characterization of a vortex pair formed by shock passage over a light-gas inhomogeneity. Journal of Fluid Mechanics 258, 217--244.